Oxyanion doping strategies to enhance the ionic conductivity in Ba2In2O5

Shin, Jaegil; Orera, A; Apperley, DC; Slater, Peter

Link to publication on Research at Birmingham portal

Oxyanion doping strategies to enhance the ionic conductivity in $Ba_2In_2O_5$

J.F. Shin[1], A. Orera[2], D.C. Apperley[3], P.R. Slater[1]*

[1]School of Chemistry, University of Birmingham, Birmingham. B15 2TT. UK

[2] Instituto de Ciencia de Materiales de Aragón, C.S.I.C.-Universidad de Zaragoza,

E-50.009 Zaragoza, Spain

[3] Department of Chemistry, Durham University, South Road, Durham. DH1 3LE.

UK.

*Correspondence to

Dr. P.R. Slater
School of Chemistry
University of Birmingham
Birmingham B15 2TT
UK

p.r.slater@bham.ac.uk

Abstract

In this paper we report the successful incorporation of phosphate and sulphate groups into the ionic conductor, $Ba_2In_2O_5$, with the samples analysed through a combination of X-ray diffraction, NMR, TGA, Raman spectroscopy and conductivity measurements. The results show that such oxyanion incorporation leads to a conversion from an ordered brownmillerite-type structure to a disordered perovskite-type, and hence increases the conductivity at temperatures $< 800^{\circ}C$. In wet atmospheres, there is evidence for a significant enhancement of the conductivity through a protonic contribution.

Introduction

Mixed metal oxides displaying high oxide ion and/or proton conductivity have attracted considerable interest as a result of their potential application as electrolytes in technologically important devices, such as Solid Oxide Fuel Cells, oxygen/hydrogen sensors and separation membranes. The most widely studied structure-types are the fluorite and perovskite systems [1-3]. In terms of the latter, one of the most well known systems is $Ba_2In_2O_5$ which adopts the brownmillerite structure, an anion vacancy ordered variant of the perovskite structure. In this compound the oxide ion vacancies are ordered such that the room temperature structure contains alternating layers of InO_6 octahedra and InO_4 tetrahedra. This vacancy ordering leads to rather low oxide ion conductivity at low temperatures. However, at a temperature of $\approx$ 930 °C, there is a phase change from orthorhombic to tetragonal resulting in disordering of these oxygen vacancies, and a corresponding discontinuous jump in oxide ion conductivity by more than an order of magnitude [4-5]. As the temperature is increased further, the cell becomes cubic (above 1040 °C), as the oxide ion vacancies become completely disordered. As a result of the high oxide ion conductivity at elevated temperatures, there has been considerable interest in doping strategies to stabilise the highly conducting high temperature structure to lower temperatures [8-13]. In this respect, by far the most successful strategy, has proved to be doping on the In site with higher valent cations, such as Sn, Ti, V, Mo and W [8-11]. In addition to displaying high oxide ion conductivity, proton conductivity has been also reported in such systems in wet atmospheres, due to water incorporation. As noted in these earlier studies, the precise defect processes with regard to water incorporation in

3

$Ba_2In_2O_5$ are more complex than conventional perovskite systems, since the brownmillerite structure has unoccupied interstitial oxide ion sites (also referred to as structural oxide ion vacancies, V_i^X) [14, 15]. This leads to four possible defect equations for the incorporation of water (eqn 1-4), as noted by Fisher and Islam [15].

$$H_2O + V_O^{\bullet\bullet} + O_O^X \leftrightarrow 2\ OH_O^\bullet \qquad (1)$$

$$H_2O + V_i^X + O_i'' \leftrightarrow 2OH_i' \qquad (2)$$

$$H_2O + 2O_O^X + V_i^X \leftrightarrow 2\ OH_O^\bullet + O_i'' \qquad (3)$$

$$H_2O + V_O^{\bullet\bullet} + O_i'' \leftrightarrow OH_O^\bullet + OH_i' \qquad (4)$$
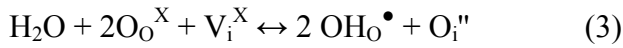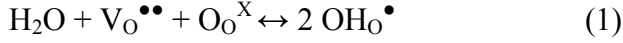
A key aspect of our recent research into improving the performance of ionic conductors has been the investigation of alternative doping strategies, in particular the possible incorporation of oxyanions, such as PO_4^{3-}, SO_4^{2-}. Our interest in this respect, stems from previous work on the incorporation of oxyanions into perovskite-type cuprate superconductors, which demonstrated that perovskite systems could incorporate significant levels of oxyanions (carbonate, nitrate, sulphate, phosphate) [16-24]. Moreover, such studies showed that this doping strategy could be used to stabilise phases, which could not be formed without doping; e.g. the Sr analogue of the high temperature superconductor, $YBa_2Cu_3O_{7-x}$ [18]. We have therefore extended this work to investigate the incorporation of oxyanions into $Ba_2In_2O_5$. Initial studies demonstrated the successful incorporation of phosphate leading to a stabilisation of the cubic cell along with enhanced conductivity below $800^\circ C$ [25]. In this paper, we report more detailed studies of these

samples, along with the synthesis and characterisation of analogous systems doped with sulphate.

Experimental

High purity $BaCO_3$, In_2O_3, $NH_4H_2PO_4$, and $(NH_4)_2SO_4$ were used to prepare $Ba_2In_{2-x}P_xO_{5+x}$ and $Ba_2In_{2-x}S_xO_{5+3x/2}$ (x = 0, 0.1, 0.2, 0.3) samples. In order to overcome Ba loss at elevated temperatures, a 3% excess of $BaCO_3$ was employed. Without this small Ba excess, low levels of Ba deficient impurity phases, such as $BaIn_2O_4$ and $Ba_4In_6O_{13}$, were observed after sintering, as has been seen in other studies synthesising similar Ba containing phases [26, 27]. The powders were intimately ground and heated initially to 1000 °C for 12h. They were then ball-milled (350 rpm for 1 hour, Fritsch Pulverisette 7 Planetary Mill) and reheated to 1000 °C for a further 50h. The resulting samples were then pressed as pellets (1.3 cm diameter) and sintered at 1300 °C for 10h. The pellets were covered in sample powder and the crucible was covered with a lid to limit the amount of Ba loss during the sintering process. Powder X-ray diffraction (Bruker D8 diffractometer with Cu Kα1 radiation) was used to demonstrate phase purity, as well as for preliminary structure determination. For the latter, the GSAS suite of programs was used [28].

In order to provide further evidence for the successful incorporation of phosphate, sulphate, Raman spectroscopy measurements were made using a Renishaw inVia Raman microscope with excitation using a Cobolt Samba CW 532 nm DPSS Laser. In addition, ^{31}P NMR data were collected to gain further information about the P environment. These

spectra were obtained using a Varian Unity Inova operating at 121.37 MHz for ^{31}P. Spectral referencing was with respect to 85% H_3PO_4.

Water contents for the hydrated samples were determined from thermogravimetric analysis (Netzsch STA 449 F1 Jupiter Thermal Analyser). Samples were heated at 10°C min^{-1} to 1000°C in N_2, and the water content was determined from the observed mass loss.

An important aspect of the work was the investigation of the effect this doping strategy has on the conductivity. The sintered pellets (>84% theoretical density) were coated with Pt paste, and then heated to 750°C for 1 hour to ensure bonding to the pellet. Conductivities were then measured by AC impedance measurements (Hewlett Packard 4182A impedance analyser) in the range from 0.1 to 10^3 kHz. Since $Ba_2In_2O_5$ displays a small but significant p-type contribution to the conductivity in oxidising conditions, measurements were made in dry N_2 to eliminate this contribution. In addition measurements were made in wet N_2 (in which the gas was bubbled at room temperature through water) to identify any protonic contribution to the conductivity.

The impedance data showed generally a single broad semicircle in dry atmospheres. The capacitance of the broad semicircle was typical of a bulk response, suggesting that in dry atmospheres, the resistance of the grain boundary is small compared to that of the bulk. In wet atmospheres, instead of the single broad semicircle, there were now two partially resolved semicircles, whose capacitances were consistent with the bulk and grain boundary respectively (see supplementary information). In the text, bulk conductivities are reported.

Results and discussion

Phosphate doped systems: $Ba_2In_{2-x}P_xO_{5+x}$ (x = 0, 0.1, 0.2, 0.3)

The X-ray diffraction data showed that undoped $Ba_2In_2O_5$ was orthorhombic as previously reported. On the incorporation of phosphate, the X-ray diffraction data showed a change from orthorhombic to cubic symmetry with increasing P content (fig. 1), and cell parameters are given in table 1. Along with the change in cell symmetry, there was a gradual reduction in cell volume (fig. 2) on phosphate incorporation consistent with the smaller size of P^{5+} compared to In^{3+} (ionic radii for 4 coordination; P^{5+} 0.17 Å, In^{3+} 0.62 Å [29]) outweighing the effect of the increased oxygen content for the doped samples. Preliminary structure refinement has been performed using the X-ray diffraction data for the highest phosphate content sample, $Ba_2In_{1.7}P_{0.3}O_{5.3}$, and this indicated B site occupancies of 1.68(1) In and 0.32(1) P, consistent with that expected (see supplementary information). Further structural characterisation using neutron diffraction data is planned to get more detailed information regarding the oxygen sites, which as shown in prior work on oxyanion containing cuprates requires the use of neutron diffraction data to fully resolve [14]. In this respect, total scattering studies would also be useful so as to resolve the separate In- and P-O distances.

The ^{31}P NMR data for the x=0.1, 0.2, 0.3 samples are given in figure 3. The data show that each contains a single broad line at a chemical shift in the region 1.4-3.0 ppm, with evidence for a small shift between samples. This chemical shift is consistent with that expected for an alkaline earth phosphate [30,31], demonstrating the presence of a PO_4^{3-}

group and suggesting a greater interaction between the phosphate group and the Ba. On hydration, there was no significant change in the ^{31}P NMR spectrum, which would suggest that the protons preferentially coordinate to oxygens on the In, consistent with the expected higher basicity of these sites.

The Raman spectra showed the emergence of bands due to phosphate at $\approx$930 cm^{-1}, which increased in intensity with increasing phosphate content (fig. 4). The bands are in a similar position to those observed for $Ba_3(PO_4)_2$, consistent with closer association with the Ba than with In, in agreement with the NMR studies. This is not unexpected, as the shorter P-O bond length when P is on the perovskite B cation site, will lead to a substantial increase in the In-O bond length to an adjacent In site. As for the ^{31}P NMR data, there was a slight peak shift (to higher wavenumber) with increasing P content.

In addition to the emergence of bands due to phosphate, the data clearly show a reduction in the the intensity of the In-O bands, most clearly seen for the bands around 600 cm^{-1}. This peak intensity reduction has been previously seen for other dopants, which introduce disorder on the oxygen sublattice. Here it should be pointed out that theoretically there should be no Raman active modes for a perfectly cubic perovskite, with the exception of possible second-order effects, and so the appearance of some bands suggests that although the average structure is cubic (as shown by XRD), there are significant local distortions away from cubic symmetry resulting in the observation of these Raman bands. The ^{31}P NMR and Raman spectra therefore clearly highlight that the P is incorporated into the structure as a phosphate group, and therefore the formula of $Ba_2In_{2-x}P_xO_{5+x}$ could also be written as $Ba_2In_{2-x}(PO_4)_xO_{5-3x}$.

Having demonstrated the successful incorporation of phosphate, the effect of this doping strategy on the conductivity was examined. The conductivity measurements showed a significant effect of phosphate doping (fig. 5). In particular, the low temperature conductivity was significantly enhanced on increasing phosphate doping, which can be correlated with the disordering of the oxygen sublattice supported by the X-ray diffraction and Raman data. At higher temperature ($>\approx 700^{\circ}$C), however, the conductivity was highest for the x=0.1 sample, with further phosphate incorporation (x=0.2, 0.3) leading to a small reduction in conductivity (fig 6). This reduction in the high temperature conductivity can be related to the fact that at these elevated temperatures all the phosphate doped samples have an oxygen sublattice in which there is significant disorder. High temperature XRD studies for the x=0.1 sample, show a significant reduction in the orthorhombic splitting, indicative of increasing oxygen disorder, above 625°C (fig. 7), which corresponds to the region where there is a steep increase in the conductivity for this sample (fig. 5). The lower conductivity for x=0.3 compared to x=0.1 in the high temperature region, could be related to the reduction in available vacant anion sites in the structure, as a result of the increase in oxygen content on phosphate incorporation, or it could be due to a small degree of vacancy defect trapping on phosphate doping.

The conductivity measurements in wet atmospheres showed a significant enhancement at temperatures $<\approx 500^{\circ}$C, consistent with a protonic contribution (table 2). In order to determine the level of water incorporation, the samples were heated under wet N_2 to 800°C, before slow cooling (0.4 $^{\circ}$C min^{-1}) to room temperature. The water content was then determined by TGA measurements. The hydration and subsequent TGA

measurements were performed in duplicate and the results showed a reduction in water content with increasing phosphate content (fig. 8). This can be explained by the fact that the starting oxygen content is increased on phosphate doping, i.e. $Ba_2In_{2-x}P_xO_{5+x}$, and hence there are less vacant sites for the accommodation of water. However, the decrease in water content is greater than expected considering simply the oxygen content, which can be explained by the tetrahedral coordination of P (in the phosphate ion), which hence precludes the filling of the other two vacant sites in the perovskite B site coordination sphere around it.

Sulphate doped systems: $Ba_2In_{2-x}S_xO_{5+3x/2}$ (x = 0, 0.1, 0.2, 0.3)

As for the phosphate doped samples, sulphate doping was also shown to lead to an increase in cell symmetry to cubic for x=0.3 (fig. 9), with cell parameters given in table 3. In this case the decrease in cell volume on sulphate incorporation is lower than that for phosphate (fig. 2), which can be correlated with the higher oxygen contents for the former partially counterbalancing the effect of the small size of S^{6+} compared to In^{3+} (ionic radii for 4 coordination; S^{6+} 0.12 Å, In^{3+} 0.62 Å [29]). Preliminary structure refinement for the x=0.3 sample, $Ba_2In_{1.7}S_{0.3}O_{5.45}$, from XRD data suggested B site occupancies of 1.73(2) and 0.27(2) for In and S respectively, consistent with those expected. As for the phosphate doped system, neutron diffraction studies are required to garner further more detailed information regarding the oxide ion sites. The Raman data were similar to those for the phosphate doped samples, with a reduction in the intensity of

the In-O bands with increasing doping levels, along with the emergence of new bands, assigned to sulphate groups in the structure (fig. 10). The positions of the main new band was similar to that of $BaSO_4$ indicating greater association of the sulphate with the Ba cations compared to the In cations, similar to the results for phosphate doping. As outlined above, the presence of Raman bands demonstrates that while the average structure is cubic, there is clearly some deviation from cubic symmetry at the local level. The Raman spectra therefore clearly highlight that the S is incorporated into the structure as a sulphate group, and therefore the formula of $Ba_2In_{2-x}S_xO_{5+3x/2}$ may also be written as $Ba_2In_{2-x}(SO_4)_xO_{5-5x/2}$.

Conductivity data in dry N_2 showed a similar enhancement in the conductivity at low temperatures on sulphate doping, consistent with the increase in disorder on the oxygen sublattice (fig. 11, 12, table 4). However, in this case, the conductivities at $400^\circ C$ were similar for x=0.1-0.3, while at higher temperatures a decrease in the conductivity was observed similar to the results from phosphate doping. Overall for the higher sulphate contents, the conductivities were slightly lower than for the related phosphate doped samples, which may be related either to the higher oxygen contents of the former, and hence lower oxygen vacancy content, or to increased defect trapping for sulphate doping. As for the phosphate doped samples, there was an enhancement of the conductivity in a wet atmosphere consistent with a protonic contribution to the conductivity. The water contents determined from TGA data were shown to be slightly lower than those for equivalent phosphate doped samples, consistent with the higher nominal oxygen content of the sulphate doped samples (fig. 8). Indeed, the effect of starting oxygen content on the

water content for both phosphate and sulphate doped samples can be clearly seen in fig. 13.

Conclusions

In summary, we have demonstrated that phosphate and sulphate groups can be doped onto the B cation site in $Ba_2In_2O_5$ leading to a transition from an orthorhombic cell to a cubic cell. As a result of the increased disorder on the oxygen sublattice, an enhancement in the low temperature oxide ion conductivity is observed, along with evidence for proton conductivity in wet atmospheres. The work highlights the potential of oxyanion doping as an alternative strategy to conventional cation doping in perovskite-related ionic conductors, and we are currently investigating such doping in SOFC electrode materials. It also raises question marks over whether carbonate incorporation may be occurring in existing perovskite electrode systems prepared by low temperature routes.

References

1. K. D. Kreuer, *Annu. Rev. Mater. Res.*, 2003**, 33**, 333.

2. J. B. Goodenough, *Annu. Rev. Mater. Res.* 2003, **33**, 91.

3. A. Orera, P.R. Slater; *Chem. Mater*. 2010, **22**, 675.

4. J. B. Goodenough, J. E. Ruizdiaz, Y. S. Zhen, *Solid State Ionics*, 1990**, 44**, 21.

5. S. A. Speakman, J. W. Richardson, B. J. Mitchell, S. T. Misture, *Solid State Ionics*, 2002**, 149**, 247.

6. G. B. Zhang, D. M. Smyth, *Solid State Ionics*, 1995**, 82**, 153.

7. T. Schober, J. Friedrich, F. Krug, *Solid State Ionics*, 1997**, 99**, 9.

8. T. Q. Ta, T. Tsuji, Y. Yamamura, *J. Alloys and Cpdss*, 2006**, 408**, 253.

9. T. Schober, *Solid State Ionics*, 1998**, 109**, 1.

10. V. Jayaraman, A. Magrez, M. Caldes, O. Joubert, M. Ganne, Y. Piffard, L. Brohan, *Solid State Ionics*, 2004**, 170**, 17.

11. A. Rolle, R. N. Vannier, N. V. Giridharan, F. Abraham, *Solid State Ionics*, 2005**, 176**, 2095.

12. K. Kakinuma, H. Yamamura, H. Haneda, T. Atake, *Solid State Ionics*, 2001**, 140**, 301.

13. H. Yamamura, Y. Yamada, T. Mori, T. Atake, *Solid State Ionics*, 1998**, 108**, 377.

14. T. Norby, Y. Larring; *Current Opinion in Solid State and Materials Science* 1997, **2**, 593.

15. C.A.J. Fisher, M.S. Islam; *Solid State Ionics* 1999, **118**, 355.

16. C. Greaves and P. R. Slater, *J. Mater. Chem.*, 1991, **1**, 17.

17. C. Greaves and P. R. Slater, *Physica C*, 1991, **175**, 172.

18. P. R. Slater, C. Greaves, M. Slaski, C. M. Muirhead, *Physica C*, 1993, **208**, 193.

19. P.R. Slater and C. Greaves; Physica C 1993, **215**, 191.

20. P.R. Slater and C. Greaves; J. Mater. Chem. 1993, **3**, 1327.

21. P.R. Slater and D.S. Wragg; J. Mater. Chem. 1999, **9**, 545.

22. Y. Miyazaki, H. Yamane, N. Ohnishi, T. Kajitani, K. Hiraga, Y. Morii, S. Funahashi, T. Hirai; *Physica C*, 1992, **198**, 7.

23. A. Maignan, M. Hervieu, C. Michel, B. Raveau ; *Physica C*, 1993, **208**, 116.

24. K. Kinochita, T. Yamada; *Nature* 1992, **357**, 313.

25. J.F. Shin, L. Hussey, A. Orera, P.R. Slater; *Chem. Commun.* 2010, **46**, 4613.

26. T. Omata, T. Fuke, S. Otsuka-Yao-Matsuo, *Solid State Ionics*, 2006**, 177**, 2447.

27. A. M. Abakumov, M. D. Rossell, O. Y. Gutnikova, O. A. Drozhzhin, L. S. Leonova, Y. A. Dobrovolsky, S. Y. Istomin, G. Van Tendeloo, E. V. Antipov, *Chem. Mater.*, 2008**, 20**, 4457

28. A.C. Larson, R.B. Von Dreele. *Los Alamos National Laboratory, Report*. No LA-UR-86-748 (1987).

29. R.D. Shannon; *Acta Cryst*. 1976, **A32**, 751.

30. G.L. Turner, K.A. Smith, R.J. Kirkpatrick, E. Oldfield; J. Mag. Reson. 1986, **70**, 408.

31. K.J.D. MacKenzie, M.E. Smith; Multinuclear Solid State NMR of Inorganic Materials; Pergamon Materials Series; v.6, 2002.

Table 1. Cell parameter data for $Ba_2In_{2-x}P_xO_{5+x}$

Sample (nominal composition)	Unit cell parameters (Å)			Unit cell volume ($Å^3$)
	a	b	c	
$Ba_2In_2O_5$	6.089(2)	16.736(8)	5.963(2)	607.6(2)
$Ba_2In_{1.9}P_{0.1}O_{5.1}$	6.055(6)	16.774(5)	5.957(7)	605.1(4)
$Ba_2In_{1.8}P_{0.2}O_{5.2}$	4.217(1)	-	-	75.0(1)
$Ba_2In_{1.7}P_{0.3}O_{5.3}$	4.208(1)	-	-	74.5(1)

Table 2. Conductivity data for $Ba_2In_{2-x}P_xO_{5+x}$

Sample (nominal composition)	Conductivity (S cm^{-1})		
	400 °C		790 °C
	Wet	Dry	
$Ba_2In_2O_5$	1.6×10^{-5}	7.6×10^{-7}	9.7×10^{-4}
$Ba_2In_{1.9}P_{0.1}O_{5.1}$	1.8×10^{-4}	1.1×10^{-5}	1.6×10^{-2}
$Ba_2In_{1.8}P_{0.2}O_{5.2}$	8.8×10^{-4}	3.9×10^{-5}	1.4×10^{-2}
$Ba_2In_{1.7}P_{0.3}O_{5.3}$	7.8×10^{-4}	5.7×10^{-5}	8.4×10^{-3}

Table 3. Cell parameter data for $Ba_2In_{2-x}S_xO_{5+3x/2}$

Sample (nominal composition)	Unit cell parameters (Å)			Unit cell volume (Å^3)
	a	b	c	
$Ba_2In_{1.9}S_{0.1}O_{5.15}$	6.007(2)	16.810(4)	6.011(5)	607.0(4)
$Ba_2In_{1.8}S_{0.2}O_{5.3}$	5.979(2)	16.843(3)	6.009(2)	605.2(2)
$Ba_2In_{1.7}S_{0.3}O_{5.45}$	4.227(1)	-	-	75.5(1)

Table 4. Conductivity data for $Ba_2In_{2-x}S_xO_{5+3x/2}$

Sample (nominal composition)	Conductivity (S cm^{-1})		
	400 °C		790 °C
	Wet	Dry	
$Ba_2In_{1.9}S_{0.1}O_{5.15}$	3.6 x 10^{-4}	3.2 x 10^{-5}	1.5 x 10^{-2}
$Ba_2In_{1.8}S_{0.2}O_{5.3}$	4.0 x 10^{-4}	2.6 x 10^{-5}	5.5 x 10^{-3}
$Ba_2In_{1.7}S_{0.3}O_{5.45}$	5.1 x 10^{-4}	3.3 x 10^{-5}	4.6 x 10^{-3}

Figure Captions

Fig. 1 X-ray diffraction patterns for $Ba_2In_{2-x}P_xO_{5+x}$: (a) x=0, (b) x=0.1, (c) x=0.2, (d) x=0.3.

Fig. 2 Variation of cubic equivalent unit cell volume with phosphate content for $Ba_2In_{2-x}P_xO_{5+x}$ (triangles), and sulphate content for $Ba_2In_{2-x}S_xO_{5+3x/2}$ (circles).

Fig. 3 ^{31}P NMR data for dry $Ba_2In_{2-x}P_xO_{5+x}$; x=0.1 (a), x=0.2 (b), x=0.3 (c). (note: the small sharp peak at ≈15 ppm is an artefact of the instrument).

Fig. 4. Raman spectra of $Ba_2In_{2-x}P_xO_{5+x}$, (a) x=0, (b) x=0.1, (c) x=0.2, (d) x=0.3, showing the emergence of bands due to the presence of phosphate (most intense band highlighted). For comparison, Raman spectra for (e) $Ba_3(PO_4)_2$ and (f) $InPO_4$ are included.

Fig. 5 Conductivity data in dry N_2 for $Ba_2In_{2-x}P_xO_{5+x}$; x=0 (open squares), 0.1 (open diamonds), 0.2 (open triangles), 0.3 (open circles). Conductivity data in wet N_2 for x=0.3 are also shown (filled circles).

Fig 6. Variation in σ_{790C} (filled circles) and σ_{400C} (open circles) in dry N_2 for $Ba_2In_{2-x}P_xO_{5+x}$. Data for σ_{400C} in wet N_2 included as open triangles.

Fig 7. Variable temperature XRD patterns for $Ba_2In_{1.9}P_{0.1}O_{5.1}$ showing a gradual reduction in orthorhombic splitting above 625°C.

Fig. 8. Water contents (n) for $Ba_2In_{2-x}P_xO_{5+x}.nH_2O$ (triangles) and $Ba_2In_{2-x}S_xO_{5+3x/2}.nH_2O$ (circles) determined from TGA data.

Fig. 9. X-ray diffraction patterns for $Ba_2In_{2-x}S_xO_{5+3x/2}$, (a) x=0, (b) x=0.1, (c) x=0.2, (d) x=0.3.

Fig. 10. Raman spectra of $Ba_2In_{2-x}S_xO_{5+3x/2}$, (a) x=0, (b) x=0.1, (c) x=0.2, (d) x=0.3, showing the emergence of bands due to the presence of sulphate (most intense band highlighted). For comparison, Raman spectra for (e) $BaSO_4$ and (f) $In_2(SO_4)_3$ are included.

Fig. 11. Conductivity data in dry N_2 for $Ba_2In_{2-x}S_xO_{5+3x/2}$; x=0 (open squares), 0.1 (open diamonds), 0.2 (open triangles), 0.3 (open circles). Conductivity data in wet N_2 for x=0.3 are also shown (filled circles).

Fig. 12. Variation in σ_{790C} (filled circles) and σ_{400C} (open circles) in dry N_2 for $Ba_2In_{2-x}S_xO_{5+3x/2}$. Data for σ_{400C} in wet N_2 included as open triangles.

Fig 13. Water contents (n) for $Ba_2In_{2-x}P_xO_{5+x}.nH_2O$ (triangles) and $Ba_2In_{2-x}S_xO_{5+3x/2}.nH_2O$ (circles) as a function of oxygen content.
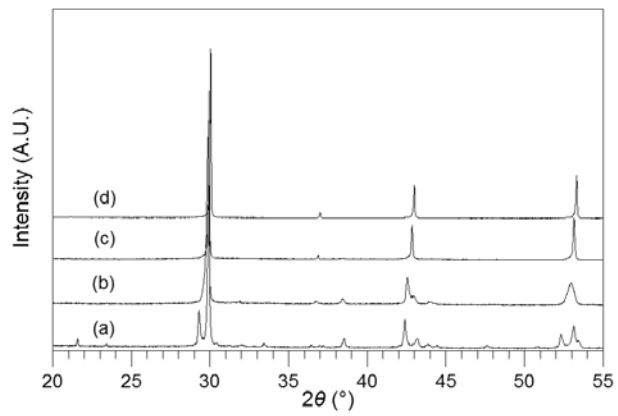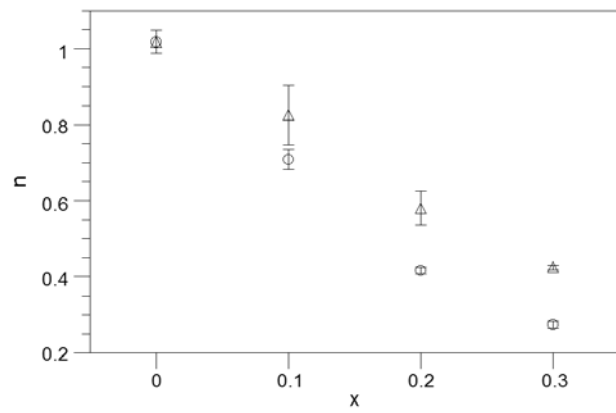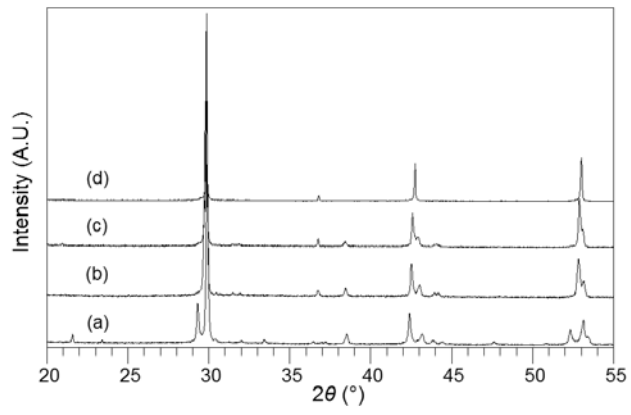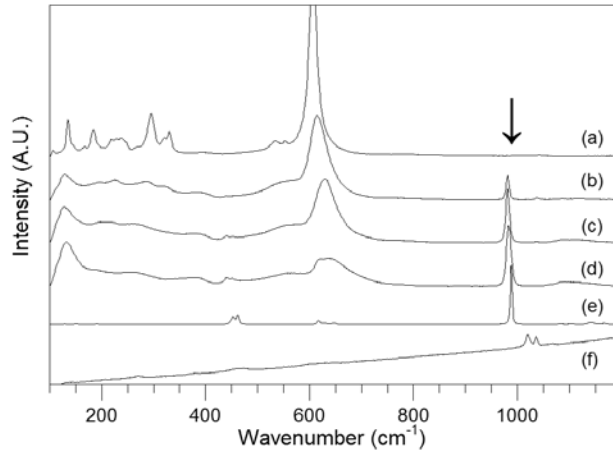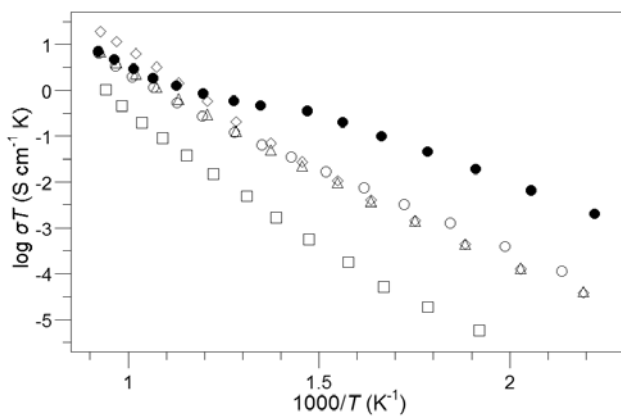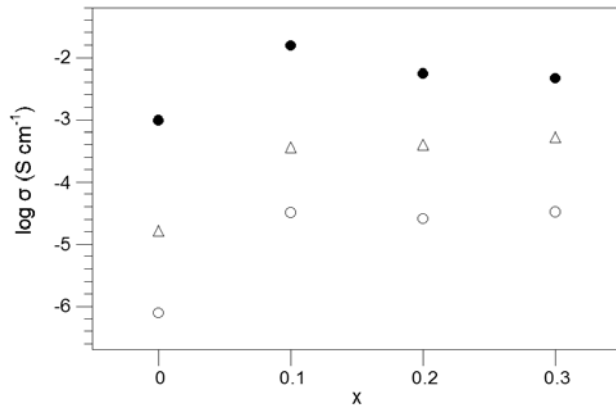
Fig. 1
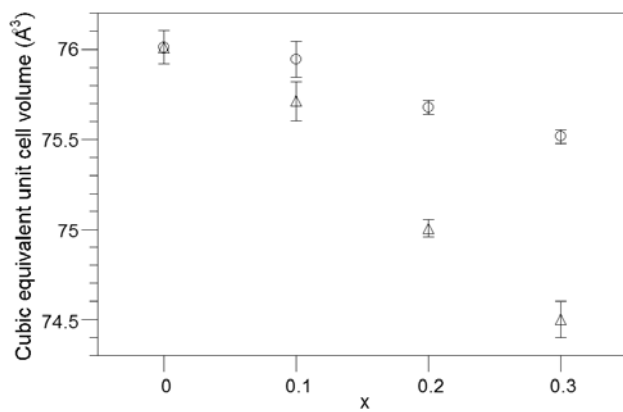
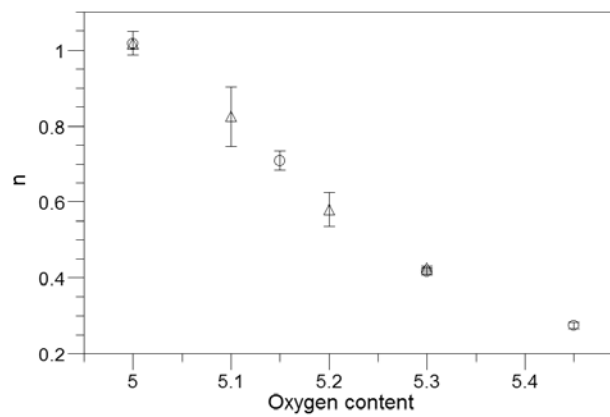Fig. 2
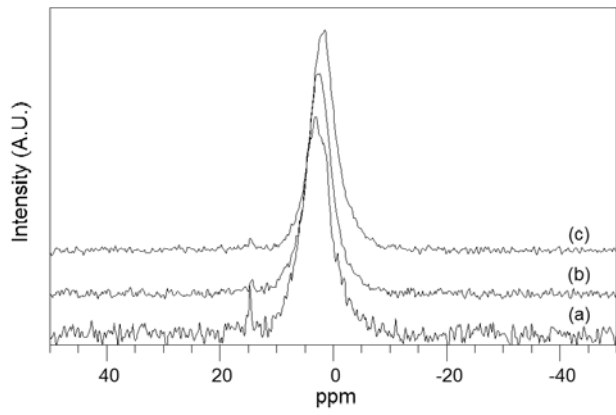
Fig. 3
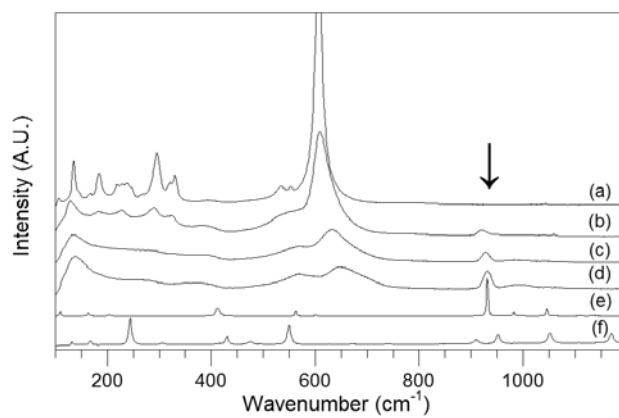
Fig. 4.
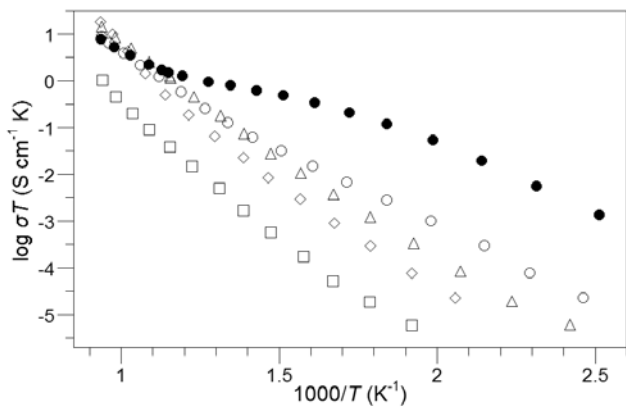
Fig. 5
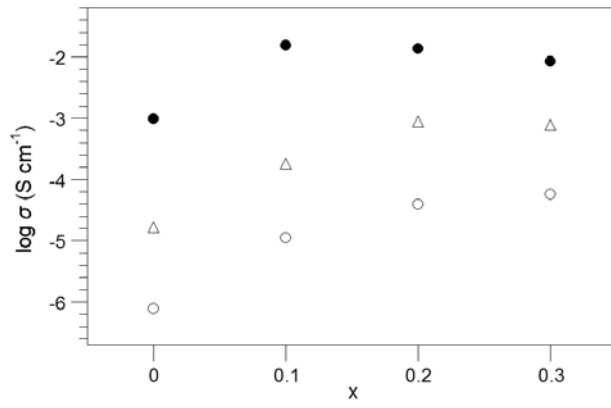
Fig 6.
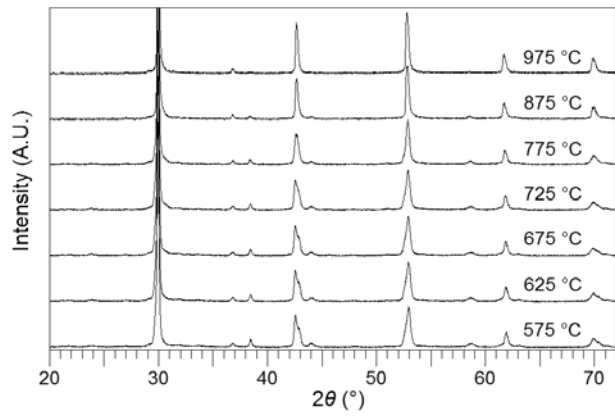
Fig 7.

Fig. 8.

Fig. 9.

Fig. 10.

Fig. 11.

Fig. 12.

Fig. 13